

QCD Matter Thermalization at RHIC and LHC

Zhe Xu¹, Luan Cheng², Andrej El¹, Kai Gallmeister³, and Carsten Greiner¹

¹Institut für Theoretische Physik, Goethe-Universität Frankfurt, D-60438 Frankfurt am Main, Germany

²Institute of Particle Physics, Huazhong Normal University, Wuhan 430079, China

³Institut für Theoretische Physik, Universität Giessen, D-35392, Germany

E-mail: xu@th.physik.uni-frankfurt.de

Abstract. Employing the perturbative QCD inspired parton cascade, we investigate kinetic and chemical equilibration of the partonic matter created in central heavy ion collisions at RHIC and LHC energies. Two types of initial conditions are chosen. One is generated by the model of wounded nucleons using the PYTHIA event generator and Glauber geometry. Another is considered as a color glass condensate. We show that kinetic equilibration is almost independent on the chosen initial conditions, whereas there is a sensitive dependence for chemical equilibration. The time scale of thermalization lies between 1 and 1.5 fm/c. The final parton transverse energy obtained from BAMPS calculations is compared with the RHIC data and is estimated for the LHC energy.

1. Introduction

Comparisons between the calculated elliptic flow v_2 from ideal (viscous) hydrodynamics [1, 2] and the measured v_2 from the experiments [3] at the BNL Relativistic Heavy Ion Collider (RHIC) support the creation of a nearly equilibrated quark-gluon system flowing with a small shear viscosity to entropy density ratio η/s . On the other hand, initially produced quarks and gluons are far from thermal equilibrium due to the subsequent rapid longitudinal expansion. How quarks and gluons thermalize within a short time scale ≤ 1 fm/c as assumed in hydrodynamical calculations is an important issue. This is not only because the thermalization time scale has to be theoretically determined, but also because the mechanism that drives the system toward equilibrium should also respond to the smallness of the η/s value and the buildup of the collective flow of the quark gluon plasma (QGP).

To investigate thermalization and collectivity in a spatially expanding particle system such like the situation in ultrarelativistic heavy ion collisions, a 3+1 dimensional parton cascade Boltzmann Approach of MultiParton Scatterings (BAMPS) [4] is developed. In this talk we will first review the role of perturbative QCD (pQCD) gluon bremsstrahlung ($gg \leftrightarrow ggg$) in thermal equilibrium and in flow buildup. Second,

new results on the initial condition dependence of thermalization and decrease of the transverse energy are given. Previous studies can be found in [5, 6].

We mention that coherent quantum effects like color instabilities [7] may play a role in isotropization of particle degrees of freedom at the very initial stage where the matter is super dense. However, more quantitative studies are needed to determine their significance on the true thermal equilibration in the expanding quark gluon matter.

2. Parton Cascade BAMPS

BAMPS solves the Boltzmann equation for partons with pQCD interactions, which include, for the moment, gluon elastic scatterings and gluon bremsstrahlung and its backreaction. The structure of BAMPS is based on the stochastic interpretation of the transition rate [4], which ensures full detailed balance for multiple scatterings. The recent numerical setup can be found in [8]. The critical energy density is set to $e_c = 0.6 \text{ GeVfm}^{-3}$. Gluons are terminated when the local energy density is smaller than e_c .

The differential cross sections and the effective matrix elements are given by [9]

$$\frac{d\sigma^{gg \rightarrow gg}}{dq_{\perp}^2} = \frac{9\pi\alpha_s^2}{(q_{\perp}^2 + m_D^2)^2}, \quad (1)$$

$$|\mathcal{M}_{gg \rightarrow ggg}|^2 = \frac{9g^4}{2} \frac{s^2}{(\mathbf{q}_{\perp}^2 + m_D^2)^2} \frac{12g^2\mathbf{q}_{\perp}^2}{\mathbf{k}_{\perp}^2 [(\mathbf{k}_{\perp} - \mathbf{q}_{\perp})^2 + m_D^2]} \Theta(k_{\perp}\Lambda_g - \cosh y) \quad (2)$$

where $g^2 = 4\pi\alpha_s$. \mathbf{q}_{\perp} and \mathbf{k}_{\perp} denote the perpendicular component of the momentum transfer and of the radiated gluon momentum in the center-of-mass frame of the collision, respectively. y is the momentum rapidity of the radiated gluon in the center-of-mass frame, and Λ_g is the gluon total mean free path, which is calculated self-consistently [4]. The interactions of the massless gluons are screened by a Debye mass $m_D^2 = \pi d_G \alpha_s N_c \int d^3p / (2\pi)^3 f/p$ where $d_G = 16$ is the gluon degeneracy factor for $N_c = 3$. m_D is calculated locally using the gluon density function f obtained from the BAMPS simulation.

The suppression of the bremsstrahlung due to the Landau-Pomeranchuk-Migdal (LPM) effect is taken into account within the Bethe-Heitler regime employing the step function in equation (2). The mean free path Λ_g serves here as an infrared regulator, which leads to a lower cutoff for the transverse momentum of the radiated (or absorbed) gluon. Compared to elastic collisions, the collision angles in a bremsstrahlung become larger due to the additional regulator [4]. This makes the $gg \leftrightarrow ggg$ processes much more efficient for kinetic equilibration. Only for large value of $\Lambda_g\sqrt{s}$, in an ultrahigh energy collision for instance, the cutoff is small and the distribution of collision angles is forwards directed, which is similar to the elastic case [10].

3. The role of $gg \leftrightarrow ggg$ in thermalization and in flow buildup

The left panel of Fig. 1 shows the momentum isotropization obtained from BAMPS calculations with a constant QCD coupling of $\alpha_s = 0.3$ for a central Au+Au collision at

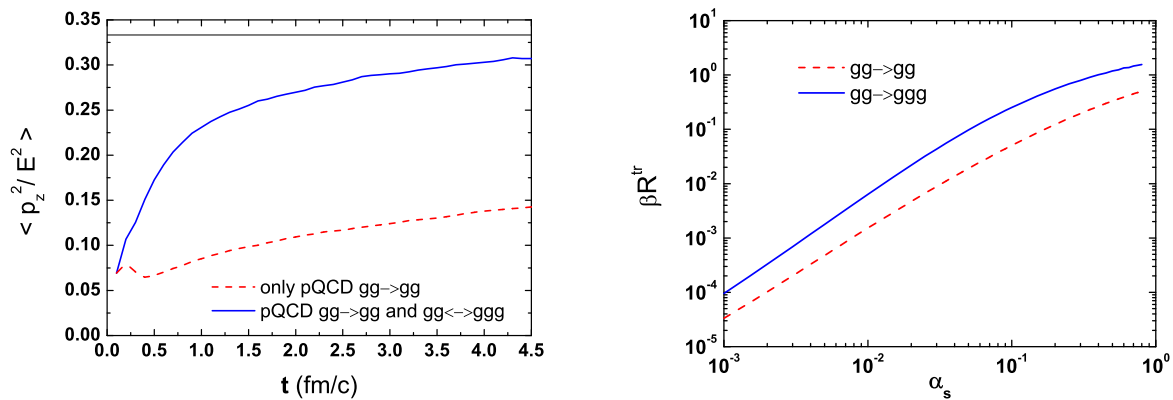


Figure 1. (color online) Left panel: momentum isotropization in the central region. Right panel: transport collision rate scaled by temperature.

$\sqrt{s_{NN}} = 200$ GeV. The initial gluon distributions are taken as an ensemble of minijets with transverse momenta greater than 1.4 GeV [10], produced via semihard nucleon-nucleon collisions with the Glauber geometry. The results of $\langle p_z^2/E^2 \rangle$ are extracted at the collision center within the space time rapidity $-0.2 < \eta_s < 0.2$ and transverse radius $x_T < 1.5$ fm. Whereas the only elastic pQCD scatterings cannot drive the system toward equilibrium, the inclusion of the gluon bremsstrahlung and its backreaction enormously speeds up the kinetic equilibration.

The large-angle distribution in bremsstrahlung is the reason for its efficiency in thermalization. Quantitatively we demonstrated that the contributions of different processes to momentum isotropization are quantified by the transport rates [10]

$$R_i^{\text{tr}} = \frac{\int \frac{d^3p}{(2\pi)^3} \frac{p_z^2}{E^2} C_i[f] - \langle \frac{p_z^2}{E^2} \rangle \int \frac{d^3p}{(2\pi)^3} C_i[f]}{n \left(\frac{1}{3} - \langle \frac{p_z^2}{E^2} \rangle \right)}, \quad (3)$$

where $C_i[f]$, functional of the gluon density distribution $f(p, x)$, is the corresponding collision term describing various interactions, $i = gg \rightarrow gg, gg \rightarrow ggg, ggg \rightarrow gg$, respectively. The sum of R_i^{tr} and that of particle drift gives the inverse of the time scale of momentum isotropization [10], which also marks the time scale of overall thermalization. The right panel of Fig. 1 shows the transport collision rate, scaled by temperature $T = 1/\beta$, for elastic $gg \rightarrow gg$ scattering and bremsstrahlung $gg \rightarrow ggg$, respectively. $R_{gg \rightarrow ggg}^{\text{tr}}$ is a factor of 3 – 5 larger than $R_{gg \rightarrow gg}^{\text{tr}}$ over a range in the coupling constant α_s from 10^{-3} to 0.8, which demonstrates the essential role of the bremsstrahlung in thermal equilibration.

In addition, the shear viscosity to the entropy density ratio η/s is inversely proportional to the sum of transport collision rate [11]. Thus $gg \leftrightarrow ggg$ processes significantly decrease the η/s value. We also found [12] that $gg \leftrightarrow ggg$ processes build up large elliptic flow v_2 observed at RHIC. When $\alpha_s = 0.3 - 0.6$ is chosen, the calculated v_2 from BAMPS is comparable with the experimental data and the extracted QGP η/s lies between 0.15 for $\alpha_s = 0.3$ and 0.08 for $\alpha_s = 0.6$.

4. Initial conditions: model of wounded nucleons and color glass condensate

To study the initial condition dependence of thermalization we choose two different types of parton initial conditions in nucleus-nucleus collisions. One is based on the model of wounded nucleons with the Glauber geometry [4]. A nucleus-nucleus collision is considered as sequent binary nucleon-nucleon collisions. To obtain the parton momentum distribution in a proton-proton collision we employ the PYTHIA event generator [13] and turn down the function of the parton fragmentation. On shell quarks and gluons are produced either by (semi)-hard parton-parton collisions or by the associated initial and final state radiations. Soft partons produced are not included to cascade calculations. To obtain initial conditions in a central Au+Au (Pb+Pb) collision the parton production in a p+p collision is scaled by a number of binary collisions N_{bin} , which is set to be $N_{\text{bin}} = 1000$. The positions of the initial partons are determined according to the nuclear overlapping density within the Glauber geometry using the Woods-Saxon profile [10]. We note that exact fractions of proton-proton, proton-neutron, and neutron-neutron collisions and shadowing effects in a nucleus-nucleus collision will be taken into account in a forthcoming paper.

Another type of initial conditions is considered as the color glass condensate (CGC) within a k_T -factorization KLN approach [14, 15, 16]

$$\frac{dN_g}{d^2r_T dy} = \frac{4N_c}{N_c^2 - 1} \int^{p_T^{\text{max}}} \frac{d^2p_T}{p_T^2} \int d^2k_T \alpha_s \phi_A(x_1, \mathbf{k}_T^2; \mathbf{r}_T) \phi_B(x_2, (\mathbf{p}_T - \mathbf{k}_T)^2; \mathbf{r}_T). \quad (4)$$

Applying such initial conditions to ideal hydrodynamic calculations final hadronic yields and their spectra measured at RHIC are well reproduced [15]. In addition, CGC initial conditions give larger initial eccentricity than the Glauber-type ones [16]. This leads to larger elliptic flow in noncentral nucleus-nucleus collisions [2]. The initial condition dependence on v_2 from BAMPS calculations will be investigated in the near future. In this work, the unintegrated gluon distribution $\phi(x, k_T^2; \mathbf{r}_T)$ is taken from Ref. [16], which, compared to the original KLN approach, gives a smooth transition from the saturation, $\phi(k_T^2) = \text{const.}$, towards the DGLAP regime, $\phi(k_T^2) \sim 1/k_T^2$. We set the prefactor for $\phi(x, k_T^2; \mathbf{r}_T)$ so that the total gluon energy is 80% of $\sqrt{s} = 200(5500)$ A GeV at RHIC(LHC), the same as obtained for quarks and gluons together in the wounded nucleons model.

5. Energy decrease and thermalization at RHIC and LHC: dependence on initial conditions

The left panel of Fig. 2 shows the momentum rapidity distribution of transverse energy of initial quarks and gluons produced in wounded nucleons model (wn) and CGC approach in a central Au+Au collision at RHIC. The transverse energy of CGC gluons is larger than that of quarks and gluons from wn model over a wide range of rapidity except for at large rapidity $|y| > 4$. The difference stems from the different approach for the production of gluons with low transverse momentum: Whereas the CGC gives

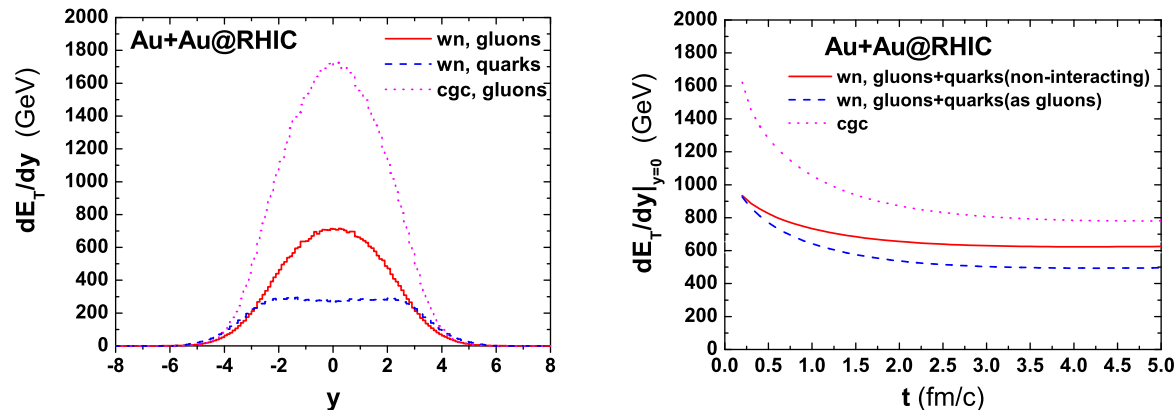


Figure 2. (color online) Left panel: momentum rapidity distribution of transverse energy of initial quarks and gluons in a central Au+Au collision at RHIC. Right panel: time evolution of the total transverse energy at midrapidity.

a moderate yield (even though suppressed due to the saturation), no production is expected in the wn model below a scale of $p_T = 1.4 - 2$ GeV, below which the pQCD parton scatterings is no longer valid.

The right panel of Fig. 2 shows the decrease of the transverse energy at midrapidity calculated from BAMPS simulations using $\alpha_s = 0.3$. For both types of initial conditions a formation time for each parton is introduced as $\tau_0 = 0.15 \cosh y$ fm/c, where 0.15 fm/c is the overlapping time of a Au+Au collision. The solid curve depicts the result when quarks in the wn model do not interact, while the dashed curve depicts the result when quarks interact as strong as gluons. The implementation of real pQCD quark dynamics in BAMPS calculations is in progress. We expect that the true final transverse energy of quarks and gluons will lie between the final values of the solid and dashed curve and thus will be comparable with the experimental data including hadronic and electromagnetic components, $dE_T/dy|_{y=0} = 620 \pm 33$ GeV [17].

The final transverse energy of CGC gluons is about 30% larger than the experimental data due to the larger initial value compared with that in the wn model, although the E_T decrease of CGC gluons is slightly stronger. To match the experimental data, a smaller critical energy density e_c has to be taken to have a later kinetic freezeout, or a larger coupling α_s has to be assumed, which will lead to a smaller η/s of the QGP. Although the latter will contradict the findings from recent viscous hydrodynamic calculations [2], new analyses with experimental data show that the extracted η/s with CGC as the initial conditions is indeed smaller than that with the Glauber-type approach [18]. Further comparisons between different extraction models have to be made.

The local momentum isotropization, $\langle p_z^2/E^2 \rangle(t)$, is shown in the left panel of Fig. 3. The solid curve depicts the momentum isotropization of gluons in the wn model, while the dashed curve depicts the result including quarks that are assumed to interact as gluons. Both curves are almost identical. This indicates that the sum of the transport collision rates R^{tr} (3), which determines momentum isotropization [10], is the same in

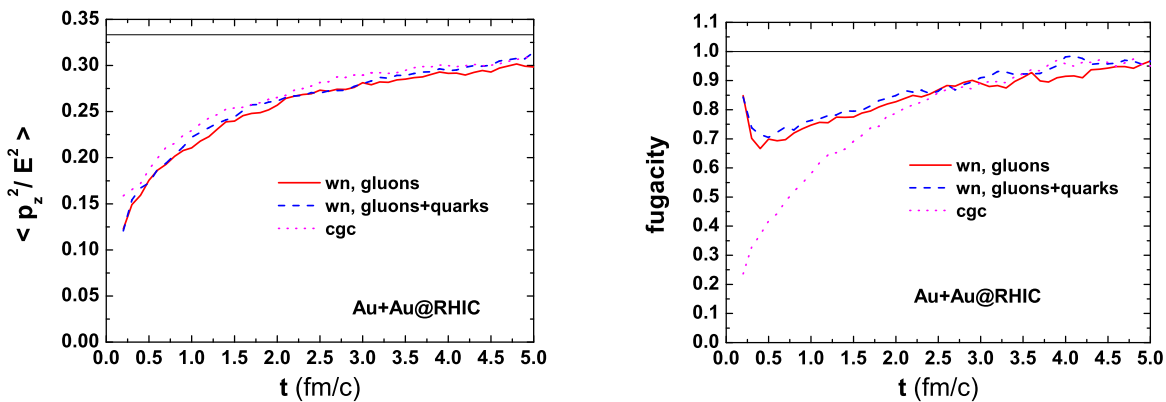


Figure 3. (color online) Momentum isotropization (left) and time evolution of the fugacity (right) in the central region in central Au+Au collisions at RHIC energy.

the QCD matter with or without quarks.

The momentum isotropization of the CGC gluons (dotted curve) is slightly faster than that of partons in the wn model. Since the initial energy density of the CGC gluons is larger (see the left panel of Fig. 2), the local effective temperature $T = e/(3n)$ is also larger than that in the wn model. This leads to a larger R^{tr} , because R^{tr} is approximately proportional to T [10]. In any case, the momentum isotropization with the initial conditions from the wn and CGC approach is not much different from that with minijets initial conditions shown in the left panel of Fig. 1. The time scale of the momentum isotropization (kinetic equilibration) is about 1.5 fm/c.

The chemical equilibration is described by the time evolution of the fugacity $\lambda(t) = n(t)/n_{eq}(t)$, where n is the local particle density and $n_{eq} = d_G T^3/\pi^2$ is the value at thermal equilibrium. The chemical equilibration shown in the right panel of Fig. 3 is quite different between the wn and CGC approach. Whereas quarks and gluons in the wn model is initially almost in chemical equilibrium, the CGC gluons need a time of 2 fm/c to achieve the chemical equilibrium.

The rapidity distribution of the initial transverse energy in central Pb+Pb collisions at Large Hadron Collider (LHC) is shown in the left panel of Fig. 4. The difference between two types of initial conditions is smaller compared to the case at RHIC, because the saturation scale Q_s of the CGC becomes larger at higher energy collisions and gluon production below Q_s is suppressed.

We perform BAMPS calculations using $\alpha_s = 0.2$ and the formation time $\tau_0 = 0.15 \cosh y$ fm/c. The final transverse energy at midrapidity is estimated to be between 1620 and 2150 GeV (see the right panel of Fig. 4). The notion “wn” in the figure implies calculations including quarks, which are assumed to behave as gluons. Note that the choices for α_s and τ_0 are crucial assumptions. With larger α_s and smaller τ_0 the decrease of the transverse energy becomes stronger.

Figure 5 shows the kinetic (left panel) and chemical (right panel) equilibration at the collision center of central Pb+Pb collisions at LHC. Similar to the case at RHIC,

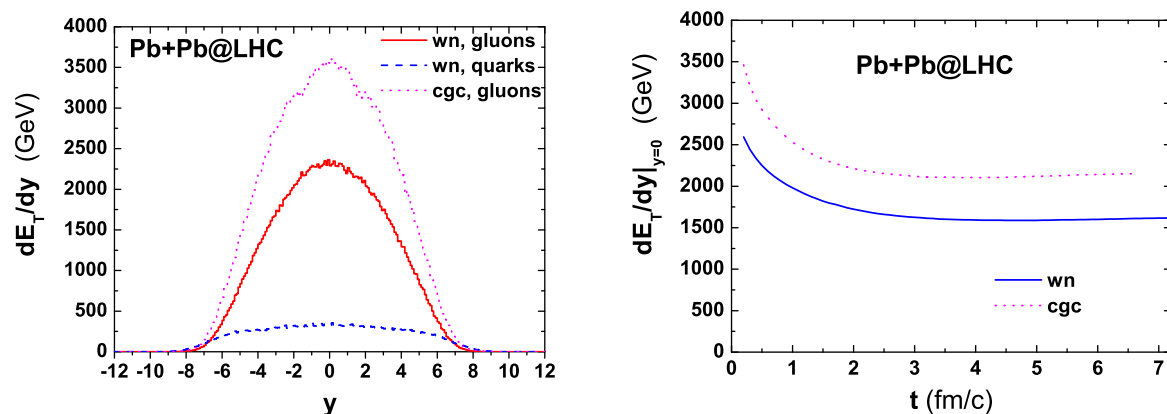


Figure 4. (color online) Same as Fig. 2 but for central Pb+Pb collisions at the LHC energy $\sqrt{s} = 5500A$ GeV with $\alpha_s = 0.2$.

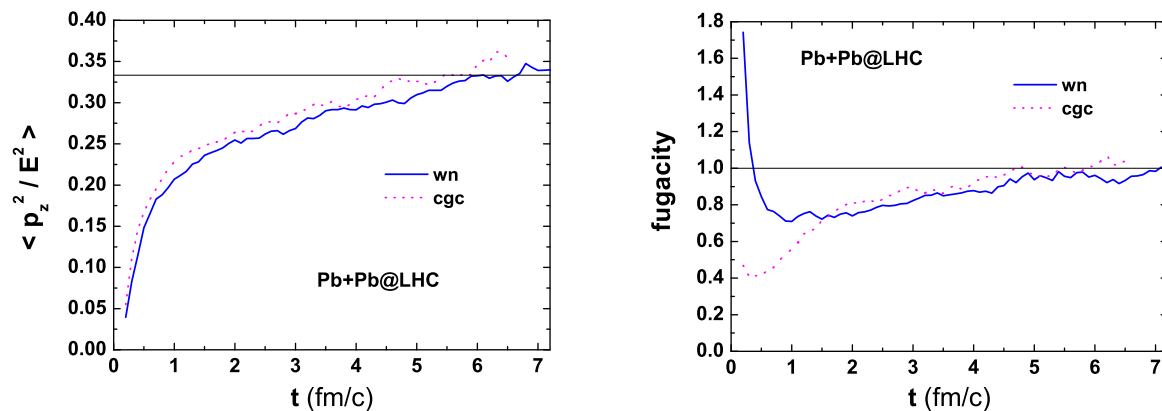


Figure 5. (color online) Same as Fig. 3 but for central Pb+Pb collisions at the LHC energy with $\alpha_s = 0.2$.

there is no much difference in momentum isotropization, whereas the CGC gluons reach the chemical equilibrium at a later time. Overall thermal equilibrium is expected to be achieved at about 1 fm/c according to the relaxation formula for $\langle p_z^2 / E^2 \rangle$ [10].

6. Summary

Employing a parton cascade BAMPS we investigated thermalization of the QCD matter produced in central nucleus-nucleus collisions at the RHIC and LHC energy. The transport collision rate is a proper quantity describing kinetic equilibration and separates contributions from various interactions. We found the QCD inspired bremsstrahlung is the dominant process in thermal equilibration and in flow buildup.

We studied the dependence of thermalization on initial conditions within the wounded nucleons model and the CGC approach. Using the same value of α_s the momentum isotropization is almost independent on the initial conditions, whereas CGC

gluons reach chemical equilibrium at a later time than partons in the wn model. On the other hand, the final transverse energy of CGC gluons is higher than that in the wn model due to their initial difference. A larger α_s for CGC gluons will accelerate the decrease of the transverse energy to reach a comparable value with the experimental data. This will also accelerate thermalization of CGC and will lead to a smaller η/s ratio. Detailed study including real quark dynamics and connecting the initial condition dependence of the buildup of elliptic flow v_2 will be done in the near future.

Acknowledgments

The authors are grateful to H.-J. Drescher and A. Dumitru for fruitful discussions and to the Center for the Scientific Computing (CSC) at Frankfurt for the computing resources. This work was supported by BMBF, DAAD, DFG, GSI and by the Helmholtz International Center for FAIR within the framework of the LOEWE program (Landes-Offensive zur Entwicklung Wissenschaftlich-ökonomischer Exzellenz) launched by the State of Hesse.

References

- [1] Huovinen P *et al* 2001 *Phys. Lett. B* **503** 58; Romatschke P and Romatschke U 2007 *Phys. Rev. Lett.* **99** 172301; Dusling K and Teaney D 2008 *Phys. Rev. C* **77** 034905; Song H and Heinz U W 2008 *Phys. Rev. C* **77** 064901.
- [2] Luzum M and Romatschke P 2008 *Phys. Rev. C* **78** 034915.
- [3] Adler S S *et al.* (PHENIX Collaboration) 2003 *Phys. Rev. Lett.* **91** 182301; Adams J *et al.* (STAR Collaboration) 2004 *Phys. Rev. Lett.* **92** 052302; Adams J *et al.* (STAR Collaboration) 2005 *Phys. Rev. C* **72** 014904; Back B B *et al.* (PHOBOS Collaboration) 2005 *Phys. Rev. C* **72** 051901(R); Adare A *et al.* (PHENIX Collaboration) 2007 *Phys. Rev. Lett.* **98** 162301.
- [4] Xu Z and Greiner C 2005 *Phys. Rev. C* **71** 064901.
- [5] Xu Z and Greiner C 2006 *Eur. Phys. J. A* **29** 33.
- [6] El A, Xu Z, and Greiner C 2008 *Nucl. Phys. A* **806** 287.
- [7] Mrówczyński S 1993 *Phys. Lett. B* **314** 118; 1994 *Phys. Rev. C* **49** 2191; 1997 *Phys. Lett. B* **393** 26; Arnold P, Lenaghan J, and Moore G D 2003 *JHEP* **0308**, 002; Arnold P *et al.* 2005 *Phys. Rev. Lett.* **94** 072302; Rebhan A, Romatschke P, and Strickland M 2005 *Phys. Rev. Lett.* **94** 102303; Dumitru A and Nara Y 2005 *Phys. Lett. B* **621** 89; Schenke B *et al.* 2006 *Phys. Rev. D* **73** 125004.
- [8] Xu Z and Greiner C e-Print: arXiv:0811.2940.
- [9] Biro T S *et al.* 1993 *Phys. Rev. C* **48** 1275.
- [10] Xu Z and Greiner C 2007 *Phys. Rev. C* **76** 024911.
- [11] Xu Z and Greiner C 2008 *Phys. Rev. Lett.* **100** 172301.
- [12] Xu Z, Greiner C, and Stöcker H 2008 *Phys. Rev. Lett.* **101** 082302.
- [13] Sjostrand T, Mrenna S, and Skands P 2006 *JHEP* **0605** 026.
- [14] Kharzeev D and Nardi M 2001 *Phys. Lett. B* **507** 121; Kharzeev D, Levin E, and Nardi M 2004 *Nucl. Phys. A* **730** 448 [Erratum *ibid.* **A 743** 329]; 2005 *Nucl. Phys. A* **747** 609.
- [15] Hirano T and Nara Y 2004 *Nucl. Phys. A* **743** 305.
- [16] Adil A *et al.* 2006 *Phys. Rev. C* **74** 044905.
- [17] Adams J *et al.* (STAR Collaboration) 2004 *Phys. Rev. C* **70** 054907.
- [18] Bai Y and Snellings R, these proceedings.